Available online at www.sciencedirect.com

jmr&t Journal of Materials Research and Technology

journal homepage: www.elsevier.com/locate/jmrt

Achievement of high-quality joints and regulation of intermetallic compounds in ultrasonic vibration enhanced friction stir lap welding of aluminum/steel

Tao Liu [a,b], *Song Gao* [a,b,*], *Weicheng Ye* [a,b], *Lei Shi* [c], *Sachin Kumar* [d], *Junnan Qiao* [e]

[a] *School of Mechanical Engineering, Qilu University of Technology (Shandong Academy of Sciences), Jinan, 250300, China*

[b] *Shandong Institute of Mechanical Design and Research, Jinan, 250300, China*

[c] *Key Laboratory for Liquid-Solid Structural Evolution and Processing of Materials (MOE), Shandong University, Jinan, 250061, China*

[d] *Department of Mechanical Engineering, Indian Institute of Science (IISc), Bengaluru, 560012, Karnataka, India*

[e] *Department of Mechanical Engineering, Tsinghua University, Beijing, 100084, China*

ARTICLE INFO

Article history:
Received 18 May 2023
Accepted 26 June 2023
Available online 3 July 2023

Keywords:
Friction stir welding
Ultrasonic assistance
Aluminum alloy
Steel
Mechanical properties
Microstructure

ABSTRACT

The lap joints of 6061-T6 aluminum alloy/Q235 steel were obtained by conventional friction stir welding (FSW) and ultrasonic vibration enhanced friction stir welding (UVeFSW). The weld forming characteristics and microstructure differences of the joints with or without ultrasonic were compared and analyzed, and the effects of acoustic energy on the mechanical properties and intermetallic compounds (IMCs) layer of the joints were revealed. The results showed that ultrasonic vibrations could effectively improve the weld surface forming quality, increase the volume of plastic flow materials, significantly improve the welding speed of defect-free joints and expand the welding process window. The additional ultrasonic vibration can refine the grain structure of the weld nugget zone and the thermo-mechanically affected zone, improve the mechanical properties of the lap joints, and change the joint's fracture position and fracture mechanism. The assistance of acoustic can significantly enhance the mechanical interlocking ability of the center of the lap interface and change the type and thickness of the IMCs layer.

1. Introduction

In modern automobile manufacturing, using aluminum alloy with lower density to replace heavier steel structures was one of the effective strategies to reduce vehicle weight and carbon emissions [1]. Therefore, how to achieve a high-quality connection between aluminum alloy and steel has become an urgent problem to be solved. When Al/steel is welded by traditional fusion welding technology, a series of solidification

* Corresponding author.
E-mail address: gaosongedu@163.com (S. Gao).

https://doi.org/10.1016/j.jmrt.2023.06.251

defects will occur because of the two materials' significant differences in thermophysical properties (melting point, density, linear expansion coefficient, and thermal conductivity) [2]. There was a considerable heat input in the welding process, which formed a thicker intermetallic compounds (IMCs) layer (usually brittle and hard) at the interface and seriously deteriorated the mechanical properties of the joints [3]. Friction stir welding was a new solid-phase bonding technology that has been rapidly developed since the beginning of the 21st century [4,5]. Compared with traditional fusion welding, the temperature of FSW was lower, inhibiting the formation of IMCs at the interface [6,7]. At present, FSW technology has become one of the main methods to realize high-quality Al/steel dissimilar metal connections [8–12].

However, in conventional FSW, to realize the strong connection of aluminum/steel dissimilar metal, the pin tool tip was usually inserted into the steel, leading to a shorter service life of the pin tool [13], and a large number of IMCs will be formed at the Al/steel interface under high heat input welding parameters, which will cause the joint to break under stress [14,15]. Helal et al. [16] reported that when the welding parameters were 1200 rpm and 50 mm/min, an IMCs layer with a thickness of 5.824 μm was formed at the Al/steel interface. This IMCs layer reduces the strength of the lap joint, and the failure load was only 2856 N. Wei et al. [17] used FSW technology to weld aluminum alloy and stainless steel, finding that the lower the welding speed, the thicker the IMCs layer. When the rotation and the welding speeds were 950 rpm and 60 mm/min, respectively, the maximum thickness of the IMCs layer reached 3.23 μm.

In order to inhibit the formation of IMCs, improve the metallurgical bonding ability of aluminum/steel dissimilar metal interface, and increase the joint failure load, researchers developed temperature-controlled external auxiliary FSW. Derazkola et al. [18] conducted welding experiments underwater (water temperature 0 °C, 25 °C, and 50 °C, respectively) and in the air, and studied the effect of different cooling media on the thickness of the IMCs layer. The results show that the IMCs layer formed in the air was the thickest, about 12 μm. With the decrease in water temperature, the thinner the IMCs layer was. When the water temperature was 0 °C, the thickness of the IMC layer was close to zero. Eyvazian et al. [19] found that compared with conventional FSW, underwater friction stir welding formed a thinner IMC layer at the joint interface. Underwater FSW restrains the growth of IMCs by reducing the peak temperature in the welding process. Tang et al. [20] studied the effect of preheating on the temperature distribution and material flow of 6061 aluminum alloy and E235 steel in Friction stir welding. The results showed that preheating treatment reduced the cooling rate of the steel after welding, significantly promoted the plastic flow of the material, reduced the flow rate difference between aluminum alloy and steel, and increased the failure load of the joint after preheating treatment from 226 MPa to 283 MPa. Liu et al. [21] realized the connection of 6061 aluminum alloy and TRIP780 steel using a new electrically assisted friction stir welding method. It was found that the addition of electrically significantly reduced the axial force during the welding process, resulting in a large number of micro interlocking structures at the aluminum/steel interface, which suppressed the generation and propagation of cracks in brittle IMCs and improved the mechanical properties of the joint. Bang et al. [22] used GTAW assisted Friction stir welding to weld 6061-T6 aluminum alloy and STS304 stainless steel. The test shows that the joint strength of GTAW assisted Friction stir welding under different welding parameters is significantly higher than that obtained by conventional FSW. The preheating effect of GTAW on the surface of stainless steel enhances the plastic flow of materials and the partial annealing effect of dissimilar materials, leading to a significant increase in the elongation of weld joints, which improves joint strength. In addition to temperature-controlled external auxiliary FSW, mechanical structured external auxiliary FSW was also a focus of attention for researchers. Huang et al. [23,24] achieved self riveting friction stir lap welding of 6082-T6 aluminum alloy and QSTE340TM steel and studied the effect of the diameter of the preset holes on the joint strength. It was found that the shear strength of the joint first increases and then decreases with the increase of the diameter of the preset hole and reaches the maximum value of 317 N/mm when the diameter of the preset hole was 3 mm. However, the above methods have some shortcomings, such as complex operation and high cost, so they can not be widely used in practical production.

To achieve a reliable connection of Al/steel structures, ultrasonic vibration (UV) was used as auxiliary energy in FSW. During the test, it was found that UV had a noticeable effect on improving the quality of the Al/steel joint. Thomä et al. [25] realized butt welding of aluminum alloy and steel by ultrasound enhanced FSW (USE-FSW). The results showed that UV could enhance the mixing degree of materials in the weld nugget zone and make more fine steel particles enter the interior of aluminum alloy. According to the observation of the Al/steel interface, it was found that the thickness of the $FeAl_3$ generated at the conventional FSW interface was about 2.8 μm, and the thickness of the IMCs layer became 1.7 μm after applying UV, which indicates that the UV had a noticeable thinning effect on the IMCs layer. Hong et al. [26] performed the lap test of aluminum alloy and steel plates using ultrasonic assisted FSW (UaFSW). It was found that conventional FSW produced uneven flashes, after applying UV, the flashes became uniform, and the joint surfaces were more smooth. When the rotating speed of the FSW tool and the welding speed was 1800 rpm and 20 mm/min, respectively, the interface IMCs layer changed from 10 μ m to 6 μ m after the application of ultrasound, and the bonding capacity of the joint was increased by 27.9%.

The ultrasonic vibration enhanced friction stir welding (UVeFSW) [27,28] used in this paper can directly apply UV to the surface of an aluminum alloy plate, which is easy to operate and will not cause a waste of ultrasonic energy. When welding Al/Mg dissimilar metal, it was found that UV can restrain the growth of IMCs, thus increasing the failure load of Al/Mg dissimilar metal joint [29,30]. This study used conventional FSW and UVeFSW to realize the connection between 6061-T6 aluminum alloy and Q235 steel. The differences in weld shape and microstructure of aluminum/steel lap joints with or without UV were compared and analyzed, and the effects of UV on the mechanical properties and the IMCs of an interface of aluminum/steel dissimilar metal FSW joints were revealed.

Table 1 – Main chemical components of 6061-T6 (wt. %).

Al	Cu	Mg	Si	Fe	Ti	Mn	Zn	Cr
Bal	0.15–0.4	0.8–1.2	0.4–0.8	0.7	0.15	0.15	0.25	0.04–0.35

2. Experiment details

2.5 mm thick 6061-T6 aluminum alloy and 1.8 mm thick Q235 steel plates were selected as base materials, and the length and width of the two plates were 200 mm and 90 mm, respectively. Tables 1 and 2 show the main chemical components of these two materials. Before welding, emery paper was used to grind the surface of the two kinds of plates to a smooth surface so that the plates fit closely together. After the emery paper treatment, the plate's surface was cleaned with acetone to remove the oil and impurities on the plate's surface. The FSW tool used in the test was made of tungsten-rhenium alloy, and its morphology and size are shown in Table 3.

Fig. 1 is a welding schematic diagram, and the two materials were placed in the form of the lap joint, aluminum alloy plate on the upper side, placed on the advancing side (AS), steel plate on the lower side, placed on the retreating side (RS), and the overlapping width of the two plates was 35 mm. The UV was applied on the surface of the unwelded aluminum alloy plate through the sonotrode with an inclination angle of 40°. The horizontal distance between the position of UV and the FSW tool was 20 mm. The output power of the ultrasonic generator was 300 W, and the frequency generated by the ultrasonic generator was 20 kHz. To better explore the effect of UV, the FSW tool was inserted into the base metal at an inclination angle of 2.5°, and the shoulder was pressed into the aluminum alloy surface by 0.1 mm. At this point, the top of the pin tool was inserted into the steel plate by 0.2 mm. During the welding, the FSW tool rotated counterclockwise, the constant rotation speed (ω) of the FSW tool was 800 rpm, and the welding speed (v) varied from 25 mm/min to 150 mm/min. During the test, the welding parameters used by conventional FSW and UVeFSW were the same, and the only difference between them was whether UV was applied during the test. In the following, C was the abbreviation of conventional FSW, and U was the abbreviation of UVeFSW. For instance, C-800-25 and U-800-25 represent welds obtained by conventional FSW and UVeFSW with welding parameters of 800 rpm and 25 mm/min.

After the welding, the weld surface forming was observed and analyzed, and then the tensile shear specimens and metallographic samples were cut by a wire-cut electric discharge machine (ZJK7532A). The position and quantity of the samples are shown in Fig. 2 (a). Fig. 2 (b) shows the detailed dimensions of the tensile shear specimen. After being polished with emery paper, the metallographic samples were buffed with a 2.5 μ m diamond polishing agent to the surface without scratches, and the aluminum alloy side was etched with Keller reagent (1 ml HF+1.5 ml HCl+2.5 ml HNO_3+95 ml H_2O) for the 90 s. The steel side was etched with a nitric acid (5 mL HNO_3 + 95 mL Ethanol) reagent for 15 s. After the corrosion was completed, the macro-morphology and microstructure of the weld were photographed by a stereo microscope (Stemi DV4) and an ultra-depth three-dimensional microscope (VHX-5000), respectively. The electronic universal testing machine (WDW-100AE) was used to carry out the tensile shear test, and the constant crosshead speed was set to 1 mm/min during the test. Vickers microhardness tester (HXD-1000TMC) was used to test the microhardness at different positions of the joint. Fig. 2 (c) is a schematic diagram for testing the microhardness of aluminum/steel lap joints. The interface and fracture morphology of the Al/steel joints was characterized by a scanning electron microscope (SEM, TESCAN MIRA). The elements can be analyzed accurately by an energy dispersive spectrometer (EDS, Oxford Xplore 30).

Table 2 – Main chemical components of Q235 (wt. %).

Fe	C	Mn	Si	P	S
Bal	0.13	0.37	0.22	0.018	0.012

3. Results and discussion

3.1. *Weld formation*

Rotation speed (ω) and welding speed (v) was the main process parameters of FSW, and the change in their values significantly affects the heat input in the welding process, which leads to apparent differences in weld surface forming. Fig. 3 shows the weld surface appearance at different welding parameters. In conventional FSW, When the welding speed was low (25 mm/min), due to a large number of rotations of the FSW tool per unit distance, the heat input was higher, resulting in greater viscosity of the material, so the material adheres to the bottom of the shoulder of the FSW tool in the welding process, resulting in pronounced burrs and uneven semicircular arc on the weld surface. When the welding speed changes in the range of 50–150 mm/min, the rotation times of the FSW tool per unit distance decreased, the heat input decreased gradually, and the viscosity of the material decreased, which made the burrs disappear, but there was still an uneven semicircular arc on the weld surface. In UVeFSW, the phenomenon of burrs and semicircular arc on the weld surface was improved at the same welding speed. When the welding speed was 100 mm/min and 150 mm/min, the weld surface was smooth, without any defects, and the semicircular arc was uniform and beautiful. The difference in weld surface appearance between conventional FSW and UVeFSW shows that UV can improve the forming quality of weld surfaces by increasing the plastic fluidity and reducing the viscosity of materials [31].

Fig. 4 shows the macroscopic morphology of conventional FSW and UVeFSW welds cross-section at different welding speeds. The joint consists of the weld nugget zone (WNZ), thermo-mechanically affected zone (TMAZ), heat affected

Table 3 – Morphology and size of FSW tool.

The diameter of shoulder	The length of pin tool	The shape of pin tool	The screw thread	Diameter of pin tool
12 mm	2.6 mm	The frustum of a cone	Right-hand thread	Tip:2.1 mm Root:4.0 mm

zone (HAZ), interface zone (IZ), and base metal (BM). In the welding process, the friction heat production between the FSW tool and the workpiece and the plastic deformation heat production of the metal material makes the base metal fully softened, which leads to the material mixing at the lap interface and the formation of a "deep pit" interface. When the welding speed was lower than 150 mm/min, no visible defects were found in conventional FSW and UVeFSW lap joints, indicating that under the three groups of welding parameters, the heat input was more significant, the plastic fluidity of the material was strong, and sufficient material flow can form defect-free lap joints. When the welding speed was increased to 150 mm/min, there were tunnel defects in the interface of conventional FSW (in the red box), as shown in Fig. 5 (a). The defects at the interface were mainly caused due to the higher welding speed and relatively low heat input during the welding process, and the flow resistance of the material was more extensive so that materials could not fill the cavity formed behind the pin tool in the plastic flow state [32]. After applying UV, no visible defects were found in the interface zone, and its morphology was shown in Fig. 5 (b), which shows the sound plastic effect of ultrasound reduces the rheological stress of the material, promotes the plastic flow of the material, increases the volume of the plastic flow material, and eliminates interface tunnel shaped defects.

3.2. *Microstructure*

Fig. 6 shows the microstructure of different zone on the aluminum alloy side of conventional FSW and UVeFSW, and the joint was made of welding parameters $\omega = 800$ rpm and $v = 25$ mm/min. Fig. 6 (a) and (b) show the grain structure in the WNZ. By comparison, it was found that the grains of conventional FSW and UVeFSW were refined equiaxed grains, but the equiaxed grains of UVeFSW were more refined, and the grain distribution was more uniform. The material in the WNZ was completely dynamically recrystallized by the intense stirring of the pin tool and the action of high temperature. After the UV was applied, the strain and strain rate of the material was increased, so the grain was refined [33]. Fig. 6 (c) and (d) were grain structures in the TMAZ. It can be seen from the figure that after the application of UV, the grain size in this zone decreases obviously, and the grain distribution becomes more uniform. The change of grain structure in the TMAZ indicates that the addition of UV changes the plastic flow state of the material in the welding process and optimizes the grain structure in the TMAZ. The HAZ had no plastic deformation during the welding process, but was only affected by the thermal welding cycle, so the grain structure of the HAZ was obviously coarsened. By comparing Fig. 6 (e) and (f), it can be seen that the grain size of the HAZ had no noticeable change after UV. Fig. 6 (g) and (h) were the microstructure of aluminum alloy base metal. In FSW, the base metal was not affected by the welding process, and its grain structure did not change. After applying UV, the base metal was only slightly affected by UV, which can not change the grain size of the base metal.

3.3. *Mechanical properties*

Fig. 7 shows the failure load of the lap joints at different welding speeds. It can be seen that in conventional FSW, when the welding speed varies within the range of 25–100 mm/min, the joints failure load increases with the increase of welding speed, and at a welding speed of 100 mm/min, the failure load reached its peak (5.51 kN). As the welding speed continued to increase to 150 mm/min, the joint failure load dropped sharply to 5.23 kN, with a decrease of 5.08%, which can be seen from the local magnification diagram at the interface of Fig. 5 (a). At this time, the reduction of the failure

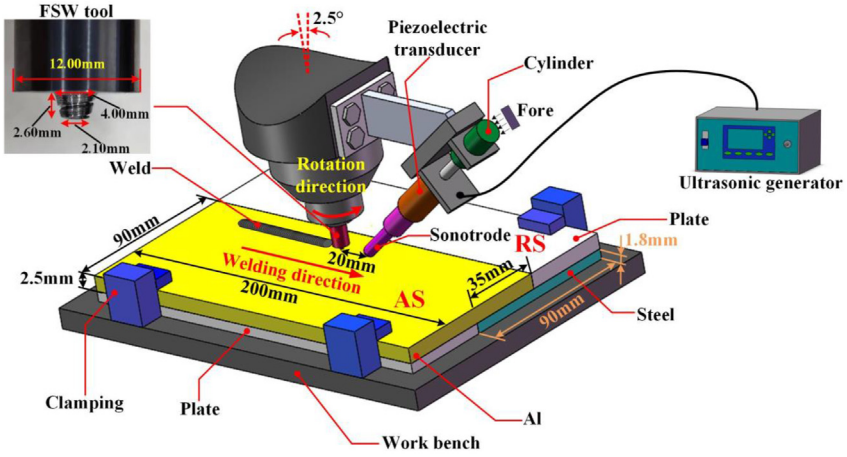

Fig. 1 – Schematic diagram of UVeFSW experimental.

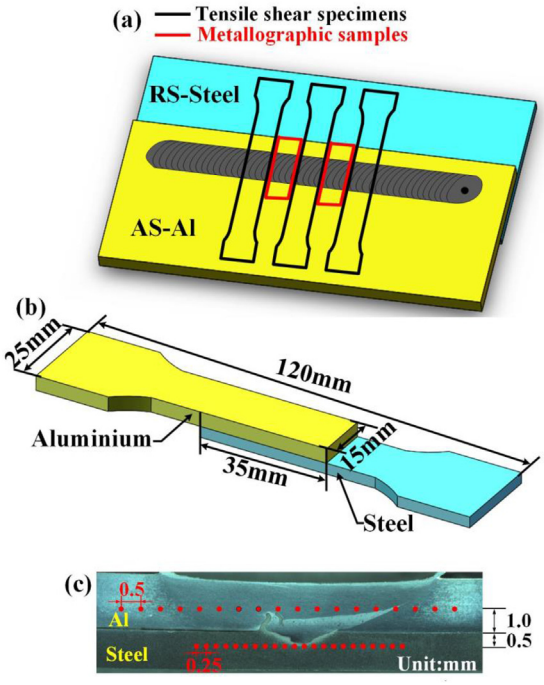

Fig. 2 – (a) Schematic diagram of the cutting position of the samples, (b) Detailed dimensions of tensile shear specimens, (c) Microhardness test location.

load of the joint was mainly caused by the tunnel defect at the interface of the lap joint. Compared with UVeFSW, the joint failure load increased gradually with the increase of welding speed in the range of selected parameters, and the variation range was 5.50 kN–6.35 kN. By comparing the failure load values of lap joints with and without UV, it can be found that UV applied to the aluminum alloy surface can significantly increase the failure load of the joints, and the maximum increase in failure load was 21.4% when the welding speed was 150 mm/min. It can be seen from Fig. 5 that the significant improvement of mechanical properties at this welding speed was because UV promoted the disappearance of tunnel defects at the interface. In the range of selected parameters, the maximum joint failure load obtained by the UVeFSW process (The failure load obtained at a welding speed of 150 mm/min was 6.35 kN) was 15.2% higher than that obtained by conventional FSW (The failure load obtained at a welding speed of 100 mm/min was 5.51 kN). After applying UV, the welding speed at the maximum failure load obtained was increased by 50%, indicating that UVeFSW provides a new idea for improving welding efficiency.

The fracture surface of the tensile shear specimen was cold embedded with resin, and the fracture position of the specimen was observed by a stereo microscope after solidification. Fig. 8 shows the fracture position of lap joints of conventional FSW and UVeFSW, obtained from the welding parameters $\omega = 800$ rpm and $v = 25$ mm/min. It can be seen from Fig. 8 that there was a "hook" structure on the AS of both conventional FSW and UVeFSW joints. When the joint was subjected to the external load, the crack propagated from the "hook" structure on the AS [14], but the fracture paths were different under the two process conditions. As can be seen from Fig. 8 (a), in a conventional FSW, the crack extends from near the "hook" structure on the AS to the center at the bottom of the WNZ and then propagates down to the IZ, eventually tearing along the Al/steel interface. It can be seen from Fig. 8 (b) that the crack initiation position of the UVeFSW specimen was at the tip of the "hook" structure on the AS. With the propagation of the fracture, the final fracture position occurs on the AS of the aluminum alloy plate, the fracture line was obviously "<" shape, and serious plastic deformation appeared on the fracture surface. It can be seen from the difference in the failure path of the joint, the conventional FSW, the weakest position of the whole joint was the bottom of the WNZ and the IZ. After applying UV, the failure position of the joint changes to the AS of the WNZ of the aluminum plate, which indicates that the addition of UV has a noticeable strengthening effect on the WNZ of the aluminum plate and IZ, and then changes the fracture position of the joint.

The fracture morphology can reflect the influence of UV on the fracture mechanism of the joints to some extent, so the fracture surface of the joints was observed and analyzed by SEM, as shown in Fig. 9. Fig. 9 (a) shows the SEM image of the conventional FSW fracture surface (the observation position is shown in Fig. 8 (a)). It can be seen from Fig. 9 (a) that the conventional FSW fracture surface shows prominent geometric characteristics of a "river pattern", with a large number of torn edges and a small number of shallow dimples, showing a ductile-brittle mixed fracture mode [34]. Fig. 9 (b) shows the SEM image of the fracture surface of UVeFSW (Fig. 8 (b) shows the shooting location). There were dimples of large size, a large number, and uniform distribution on the fracture surface of UVeFSW, which was the main feature of ductile fracture. The existence of UV promotes the plastic flow of the material and increases the mixing between the BM, thus changing the fracture mechanism of the joint (from ductile-brittle mixed fracture of conventional FSW to ductile fracture of UVeFSW).

Fig. 10 shows the microhardness curves at different positions of the joint under two welding processes at $\omega = 800$ rpm and $v = 25$ mm/min. Fig. 10 (a) shows the microhardness curve of the aluminum alloy side at a distance from the Al/steel interface 1 mm on the cross-section, and both curves show an irregular "W" shape. The value of microhardness was larger in the center of the weld, extending outward from the edge of the pin tool, the microhardness gradually reached the lowest value and then gradually increased, reaching the highest value in the position of the base metal. In the two hardness curves, the lowest point of microhardness on the AS was lower than on the RS. From the hardness curve, it can be found that the microhardness without UV varies from 52.0 HV to 62.7 HV in the range of shoulder diameter, and from 55.3 HV to 68.5 HV after UV, and the microhardness of UVeFSW was higher than that of conventional FSW. The improvement of microhardness to a certain extent shows that the strength of the WNZ of UVeFSW was higher than that of conventional FSW, which provided evidence for the change of fracture location in the previous article. The increase in microhardness on the aluminum alloy side of UVeFSW was firstly due to the reduction of the activation energy of dislocation movement by ultrasound, which leads to the formation of more

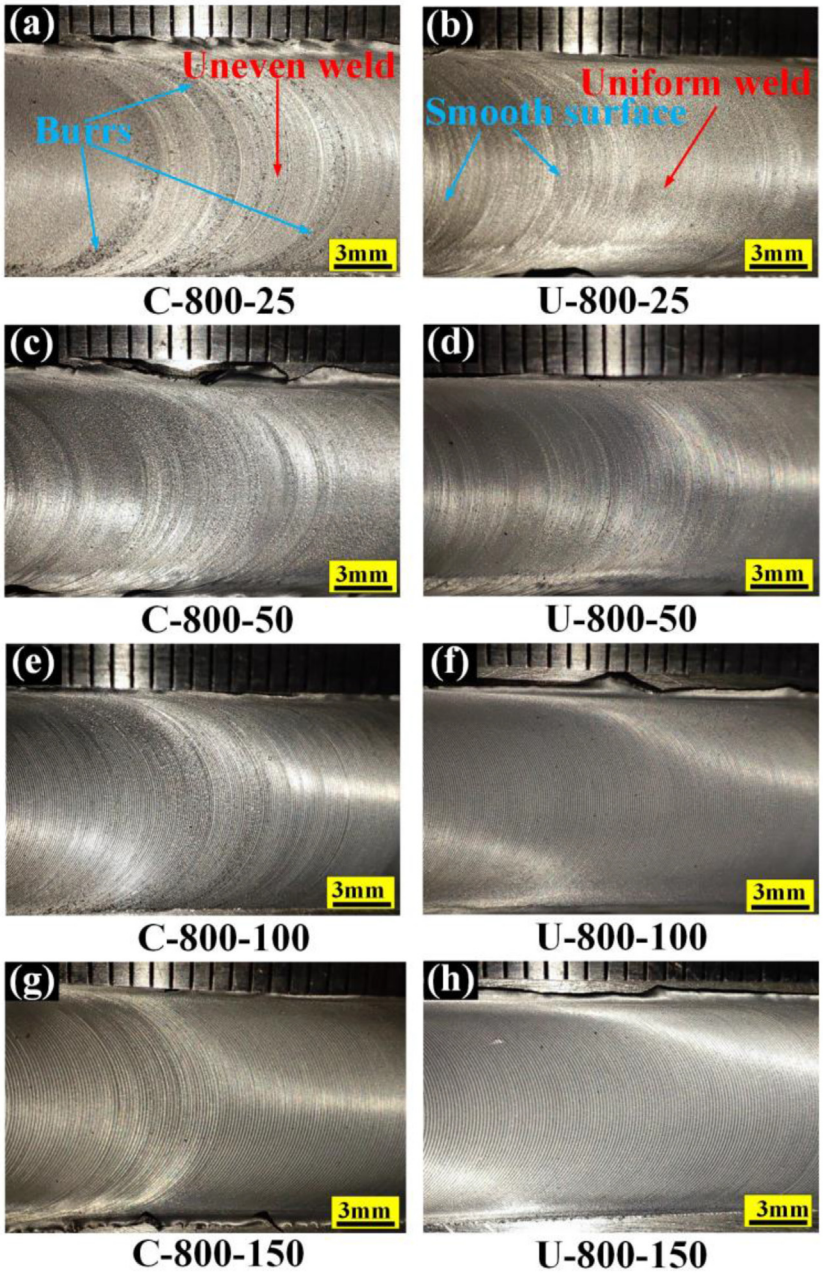

Fig. 3 – Weld surface appearance at different welding speeds.

subgrains in the weld area, thereby refining the weld grain size [35,36]. Secondly, it was speculated that ultrasound could cause an increase in vacancies, resulting in the formation of more precipitated phases in the weld after applying ultrasound [37,38]. Fig. 10 (b) shows the microhardness curve of the steel side at a distance from the Al/steel interface of 0.5 mm on the cross-section. The microhardness curve of the conventional FSW and UVeFSW steel sides had an inverted "V" profile, and the microhardness value of the weld center position was the highest. With the increased distance from the weld center, the microhardness value gradually decreases to that of the base metal. The microhardness values of conventional FSW and UVeFSW steel sides were similar, which indicates that UV had little effect on steel side microhardness during welding.

3.4. *Intermetallic compounds*

Fig. 11 shows the SEM image at the interface of the conventional FSW joint, obtained by the welding parameters with $\omega = 800$ rpm and $v = 25$ mm/min. During the welding, the steel plate was penetrated through 0.2 mm by the tip of the pin tool, so the material at the interface was vigorously stirred and extruded by the pin tool, resulting in severe plastic deformation at the interface, as shown in Fig. 11(a). It can be seen from the figure that there was a "hook" structure on both the AS and

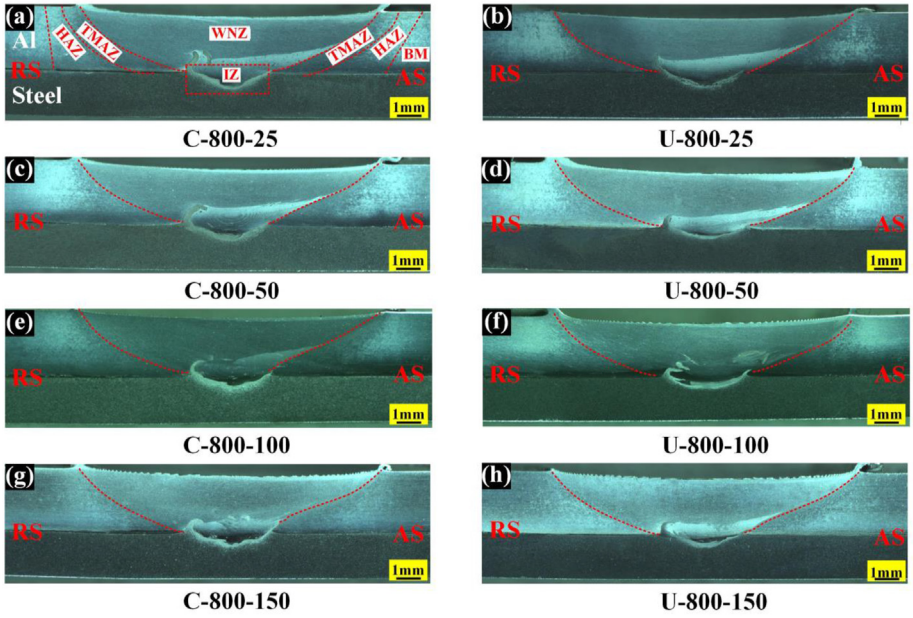

Fig. 4 – Macrostructure at different welding speeds.

the RS, and there were steel fragments (in a white circle) with an area of about 0.08 mm^2 near the "hook" structure on the RS. Combined with the morphology of the "hook" structure on the RS, it was inferred that the steel fragments were caused by the fracture of the "hook" structure on the RS, and the existence of large steel fragments was easy to produce stress concentration, which deteriorates the mechanical properties of the joint [39]. The "hook" structure on the RS breaks into massive fragments at the top, indicating that in the conventional FSW process, the friction resistance of the metal material flowing at the interface was more considerable, and the force was disordered, which leads to the unstable flow of the "hook" structure, which leads to its fracture. Due to the severe friction and extrusion of the material by the pin tool in the welding process, the steel structure below was dispersed on the aluminum alloy side in the form of particles, and the steel particles flowed from the RS to the AS on the aluminum alloy side (As indicated by yellow dotted arrow), and the distribution of steel particles was different in different positions. The number of steel particles on the RS and the central position was less, and the number of steel particles on the AS was denser, and the farthest vertical height from the Al/steel interface was 0.81 mm. It can also be found from Fig. 11 (a) that there was a large fluctuation in the position of the center of the interface, and the slope of the steel structure on the RS decreased sharply, with an angle of 75.5°, which was due to the poor plastic fluidity of conventional FSW during welding.

The mechanical stirring and thermal cycling in different interface areas were quite different, so the morphology of the interface was different. To understand the microstructure of the interface in detail, different regions of the interface of conventional FSW were photographed and analyzed by SEM and EDS. Fig. 11 (b), (c), and (d) show the microstructure of the RS, the central position, and the AS of the interface, respectively. It can be seen from Fig. 11 (b) that under the intense mechanical stirring of the pin tool, the IMCs layer with dark gray contrast was formed between aluminum alloy and steel, and the thickness of the IMCs layer varies greatly at different locations of the interface. Fig. 11 (e) was a locally enlarged image of the e region in Fig. 11 (b). The thickness of the IMCs layer was measured many times by Image J software to get the average value. It was found that the average thickness of the

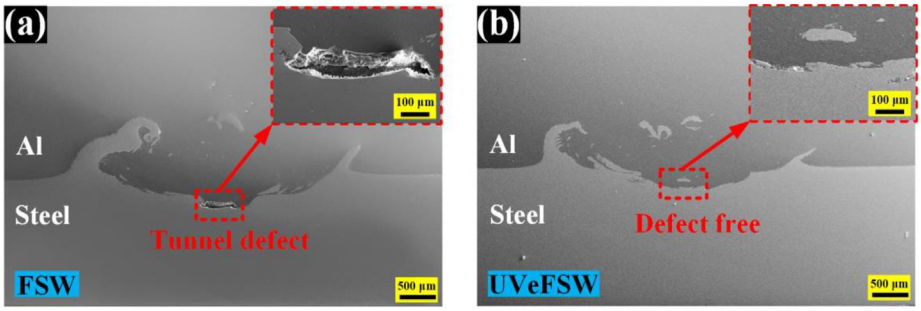

Fig. 5 – Morphology of IZ: (a) FSW, (b) UVeFSW (800–150).

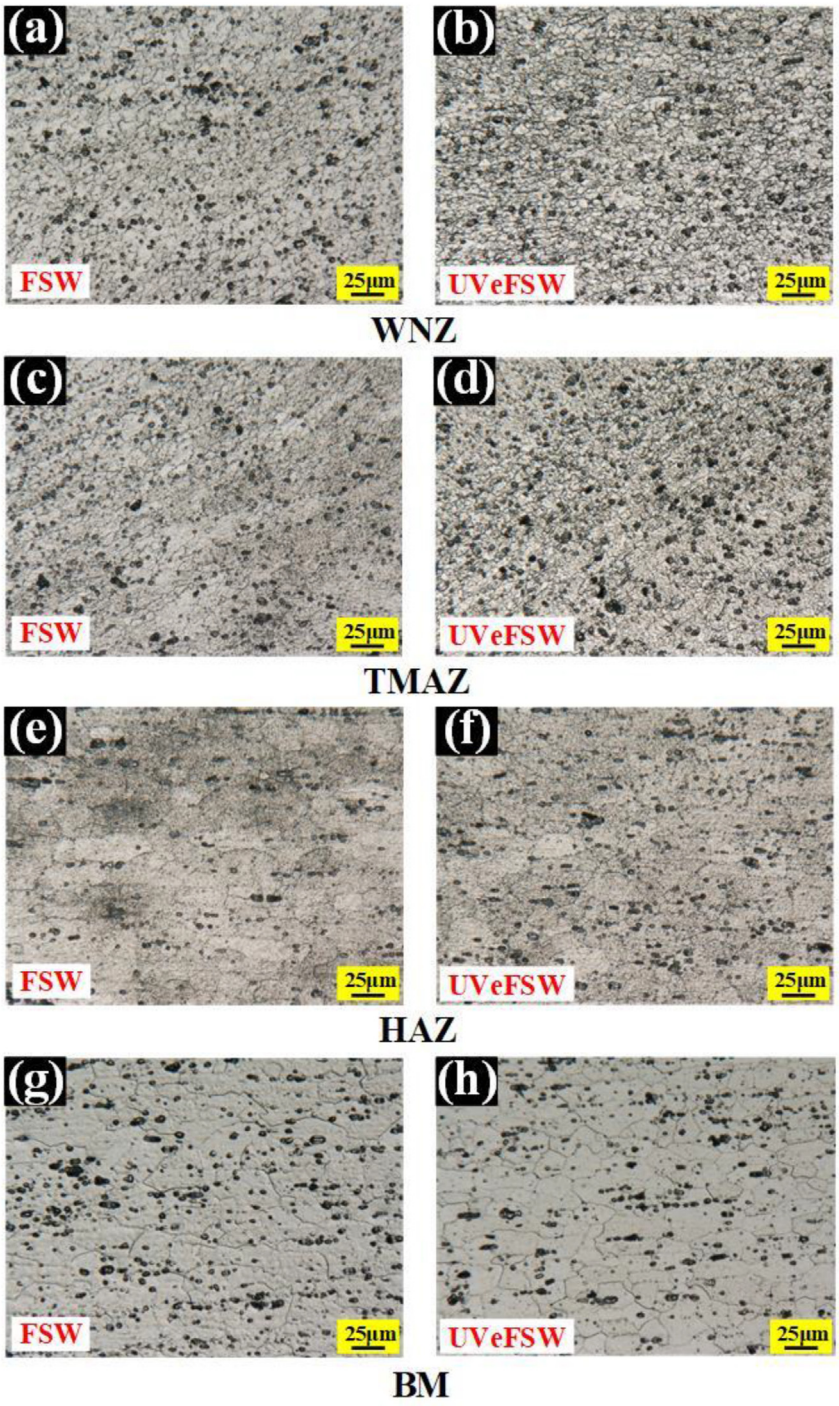

Fig. 6 – Microstructure of welded joint (800–25).

IMCs layer was about 2.31 μ m. The analysis of the IMCs layer by EDS point scanning shows that the IMCs with dark gray contrast contain 76.13 at.% element Al and 23.28 at.% element Fe. It was inferred that the type of IMCs layer was $FeAl_3$. From the central position of the interface in Fig. 11 (c), it can be seen that the Al/Steel interface was relatively straight, there was an aluminum alloy structure extruded by the pin tool on the steel side, and there was an IMCs layer with uneven thickness at the interface. According to Fig. 11 (d) and the local enlarged image of the f region (Fig. 11 (f)), it can be found that the mixing degree of the Al/steel interface on the AS was lower than that on the RS and central position of the interface, and no prominent IMCs layer was found here.

Fig. 12 shows the locally enlarged image of the C1 region in Fig. 11 (c) and the scan results of the EDS. The average thickness of the IMCs layer here was about 5.01 μ m. The interface

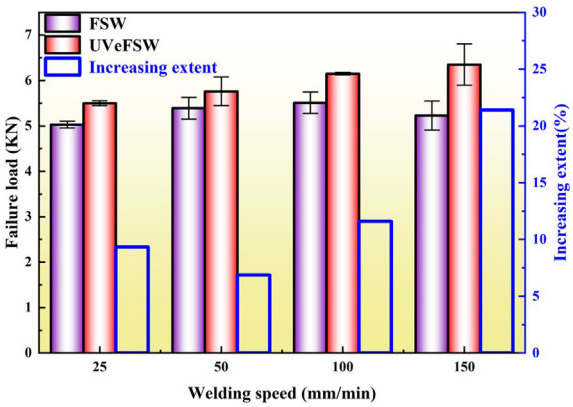

Fig. 7 – Failure loads of joints at different welding speeds.

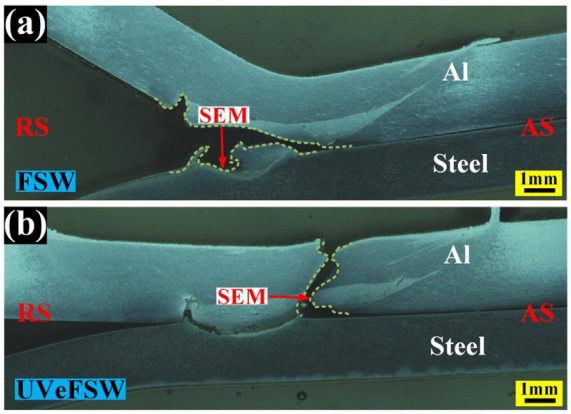

Fig. 8 – Fracture location of tensile shear specimens: (a) FSW, (b) UVeFSW (800–25).

was analyzed along the red solid line 1 by EDS line scanning. It was found that the darker structure was mainly element Al, the brighter tissue was mainly element Fe, there was a mixture of element Al and element Fe in the dark gray contrast IMCs layer, and the line scan shows a stable platform of element Al and element Fe, which indicates that there were Al/Fe intermetallic compounds with fixed composition here. The area scan by EDS shows that the mixing degree of aluminum alloy and steel was high, and new substances were formed by the element Al and element Fe at the interface. In order to determine the type of IMCs layer here, the analysis of the IMCs layer by EDS point scan shows that the IMCs layer with dark gray contrast contains 76.41 at.% elements Al and 22.30 at.% element Fe. It was inferred that the type of IMCs layer in the center of the interface was $FeAl_3$.

Fig. 13 shows the SEM morphology of the UVeFSW Al/steel lap joint interface, produced by the welding parameters of FSW tool rotation speed 800 rpm and welding speed 25 mm/min. Fig. 13 (a) shows the interface morphology of low-power SEM, which was the same as that of conventional FSW. There was a "hook" structure on both the AS and the RS of the interface, many steel particles were dispersed on the aluminum alloy side, and there was a flow trend from the RS to the AS (As indicated by the yellow dotted arrow). Compared with conventional FSW, the distribution range of steel particles in UVeFSW was more expansive, its size was smaller, and the vertical distance between the AS and the interface of steel particles reached 0.95 mm, which provides strong proof that UV promotes material flow. It can also be seen from Fig. 13 (a) that, different from the conventional FSW, the fluctuation of the position at the center of the interface was minor, and the slope of the steel structure on the RS was only 14.2°. The change in the microstructure of the steel at the center of the interface shows that UV can effectively stabilize the welding process.

The different positions of the UVeFSW interface were photographed and analyzed in detail using SEM and EDS. The RS, the central position, and the AS of the interface are shown in Fig. 13 (b), (c), and (d), respectively. It can be seen from Fig. 13 (b) that the structure of the area near the interface of the steel side was relatively complex, where aluminum alloy and steel form an IMCs layer with uneven thickness. Fig. 13 (e) shows a locally enlarged image of the e region in Fig. 13 (b). It can be seen that there was an IMCs layer with an average thickness of 0.92 μ m. Analysis was carried out by EDS point scanning, and it was found that a FeAl was composed of 52.05 at.% elements Al and 47.01 at.% element Fe. As can be seen from Fig. 13 (c), the high degree of mixing at the Al/steel interface leads to a winding at the interface, where the steel structure forms a "flow arm" inserted into the aluminum alloy (in the orange circle). The formation of the "flow arm" can enhance the mechanical interlock ability at the interface and improve the interface strength of the joint. Many small steel particles were on the aluminum alloy side, and there was a flow trend from the upper part of the AS to the lower part of the RS. As can be seen from Fig. 13 (d) and the local enlarged

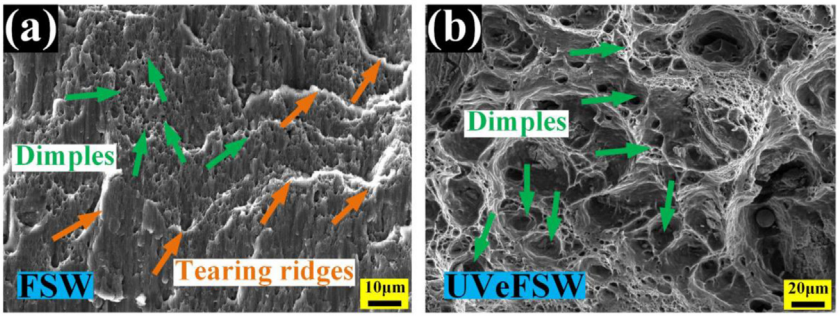

Fig. 9 – SEM image of the fracture surface: (a) FSW, (b) UVeFSW (800–25).

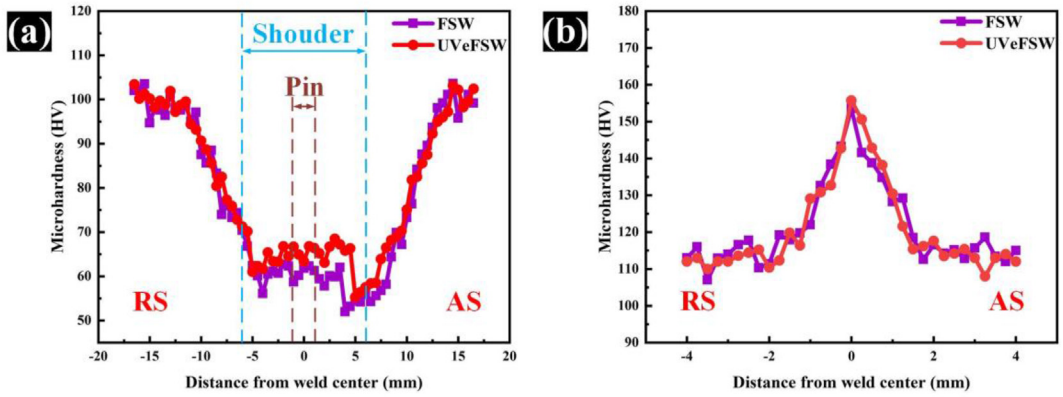

Fig. 10 – Microhardness at different positions of FSW and UVeFSW joints: (a) 6061-T6 aluminum alloy plate, (b) Q235 steel plate (800–25).

image of the f region (Fig. 13 (f)), the AS of the interface was relatively straight, and there was no prominent IMCs layer here.

Fig. 14 shows the local enlarged image of the U1 region in Fig. 13 (c) and the results of the EDS scan. Under the combined action of mechanical stirring, high temperature, and UV, the material at the interface produced mixed flow at the micro-scale, forming a complex interface composed of IMCs layer and laminated structure. The laminated structure had a solid micro-interlock effect, which can improve the strength of the Al/steel lap joint [40]. The ductility and fluidity of the steel structure were poor, and the plastic flow of the steel structure near the interface forms a long strip structure, which shows that the flow resistance of the steel structure was small and the plastic fluidity of the material was strong under the action of UV. Scanning along the red solid line 2, it was found that the element distribution at the interface was more complex, there was a transitional distribution of element Al and element Fe, and the average thickness of the IMC layer was only 0.71 μ m. By DES point scanning analysis, the IMCs layer was FeAl composed of 55.34 at.% elements Al and 44.07 at.% element Fe. The IMCs layer forms an effective metallurgical bond, which significantly improves the overall bonding strength of the interface.

The failure load of the Al/steel lap joints largely depends on the mechanical bonding and metallurgical bonding ability at the interface. Compared with the conventional FSW and UVeFSW lap joint interface, it can be found that the central position of the interface of the conventional FSW joint was relatively straight (Fig. 11 (c)), the mixing degree of the material was lower, and the mechanical bonding ability was poor. After applying UV, the flow stress in the welding process was reduced, the mixing degree of aluminum alloy and steel was improved, and the "flow arm" formed by the steel structure at the interface was inserted into the aluminum alloy (Fig. 13 (c)), and there was a laminated structure at the interface (Fig. 14),

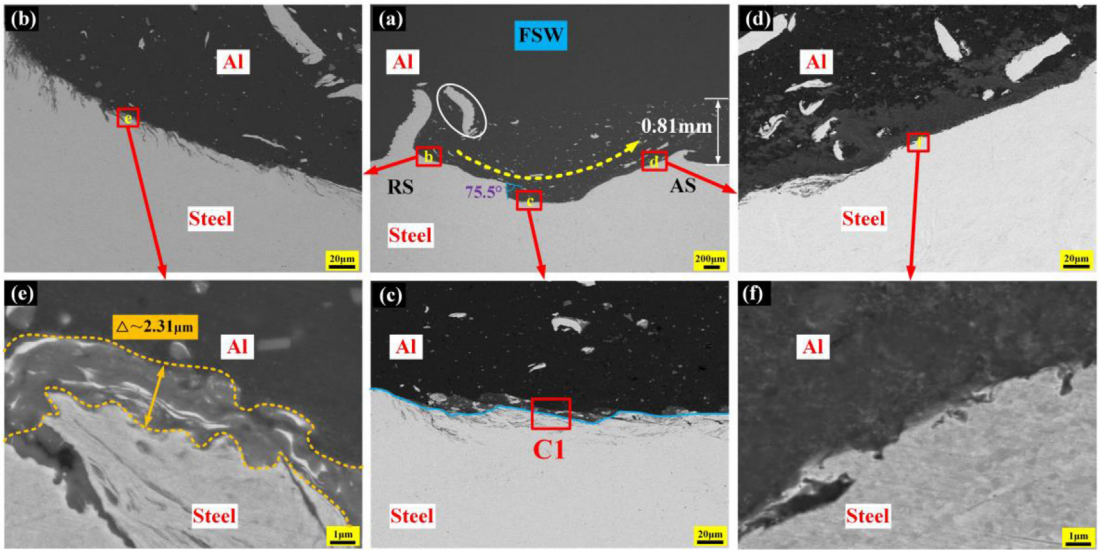

Fig. 11 – (a) SEM image in IZ of conventional FSW weld (C-800-25), (b) Morphology of the RS of the interface, (c) Morphology of central position of interface, (d) Morphology of the AS of the interface, (e) Local enlarged image of the e region in (b), (f) Local enlarged image of the f region in (d).

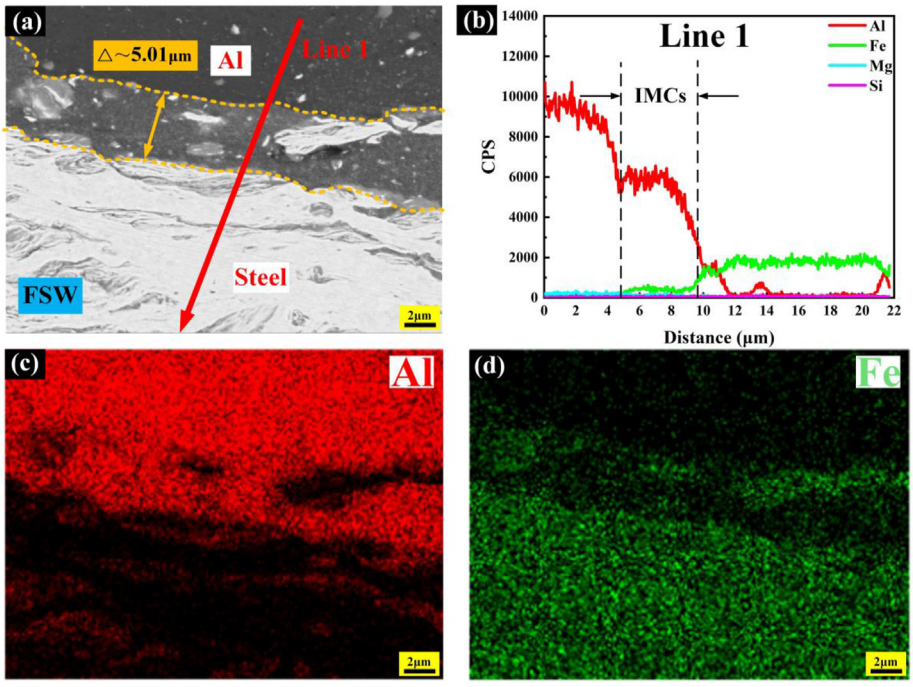

Fig. 12 – Local enlarged image of the central position of the conventional FSW interface zone and EDS results:(a) SEM image, (b) The result of EDS scanning for line 1, (c) Element Al (d) Element Fe.

which significantly improves the bonding ability of the aluminum/steel interface, thus changing the fracture location of the joint.

Severe plastic deformation occurs at the center of the interface, which enhances the diffusion ability of atoms, and leads to the formation of Al/Fe intermetallic compounds. The type and thickness of Al/Fe intermetallic compounds have a crucial influence on the bonding properties of the joints [41]. It is generally believed that Al-rich IMCs (such as $FeAl_6$, $FeAl_4$, $FeAl_3$, and $FeAl_2$) have high brittleness and are easy to crack, which leads to the deterioration of the mechanical properties of joints. Fe-rich IMCs (such as FeAl and Fe_3Al) have high toughness and can improve the interfacial bonding ability of joints. The research shows that the Gibbs free energy of the Al-rich phase was lower [42], making it easier to form the Al-rich phase in the welding process. In conventional FSW,

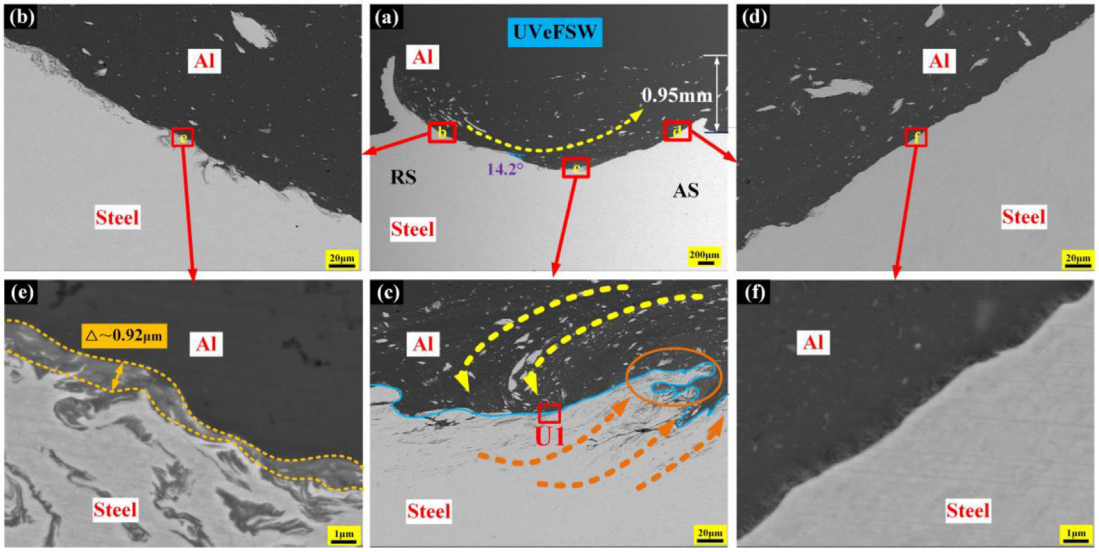

Fig. 13 – (a) SEM image in IZ of UVeFSW weld (U-800-25), (b) Morphology of the RS of the interface, (c) Morphology of central position of interface, (d) Morphology of the AS of the interface, (e) Local enlarged image of the e region in (b), (f) Local enlarged image of the f region in (d).

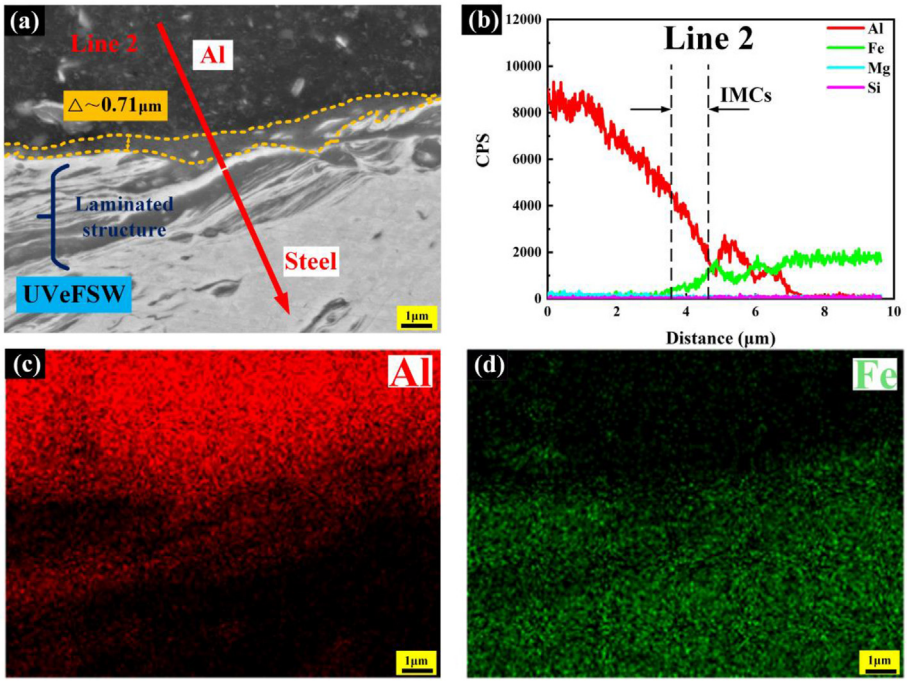

Fig. 14 – Local enlarged image of the central position of the UVeFSW interface zone and EDS results:(a) SEM image, (b) The result of EDS scanning for line 2, (c) Element Al (d) Element Fe.

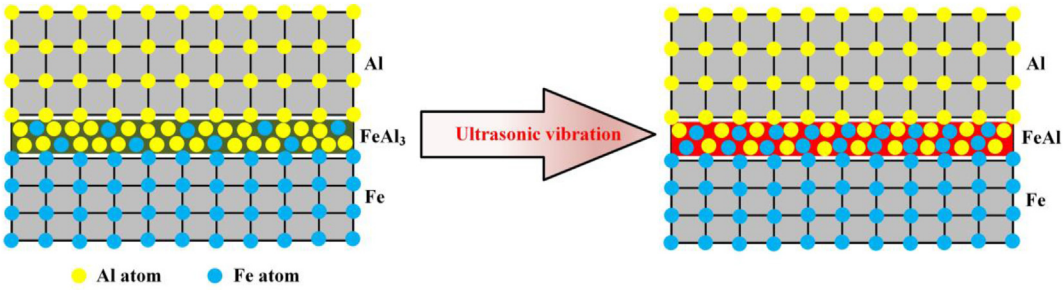

Fig. 15 – Schematic diagram of the influence of UV on IMCs layer.

$FeAl_3$ was preferentially formed and stabilized. After applying UV, the fluidity of the material was enhanced, and the diffusion coefficient of the Fe atom to the Al atom was improved. Then Fe atom reacts with preferential formed $FeAl_3$ to form FeAl with high toughness, as shown in Fig. 15. Therefore, in UVeFSW, the type of IMCs at the center of the Al/steel interface changes from $FeAl_3$ with high brittleness to FeAl with high toughness.

The thickness of the IMCs layer at the interface also significantly influences the joint's strength. When the IMCs layer was thin, the metallurgical bonding of the Al/steel interface will be realized, which will increase the strength and fatigue performance of the joints, but the excessive thickness of the IMCs layer at the interface will easily lead to cracks at the interface and reduce the bearing capacity of the joint. In UVeFSW, the thickness of the IMCs layer at the center of the interface decreases from 5.01 μm to 0.71 μm, which was speculated to be mainly caused by two reasons: on the one hand, based on previous research [43], the addition of UV can improve the plastic flow behavior of the material, reduce the heat produced during welding, accelerate the heat dissipation rate of the material, and then reduce the formation of IMCs. On the other hand, under the action of "ultrasonic-thermal-mechanics" multi-field coupling, the material had a strong plastic flow, which caused the thicker IMCs layer accumulated at the interface to be crushed into IMCs fragments, which significantly reduced the thickness of the IMCs layer [25,26].

4. Conclusions

The lap test of the 2.5 mm thick aluminum alloy plate and 1.8 mm thick steel plate was carried out. The weld forming

characteristics and microstructure differences of conventional FSW and UVeFSW were compared and analyzed, and the effects of acoustic energy on the mechanical properties and interface IMCs layer of the joint were investigated. The main conclusions are as follows.

1. The weld surface produced by UVeFSW was well-formed, and the phenomenon of burrs and uneven semicircular arc patterns had been improved. Under the acoustic softening effect of ultrasonic vibration, the internal flow stress of the material was effectively reduced, the plastic fluidity of the material was significantly improved, and the welding process window was significantly expanded.
2. Ultrasonic vibration refined the grain structure of the WNZ and TMAZ, increased the joint failure load at different welding speeds, increased the welding speed to obtain the maximum failure load, and significantly improved the welding efficiency. After the ultrasonic vibration was applied, the bottom of the WNZ and the IZ was effectively strengthened, which led to the change in the fracture position and fracture mechanism of the lap joint.
3. The assistance of acoustic can change the flow state of interface materials and improves the ability of mechanical interlock at the center of the interface. After applying ultrasonic vibration, the type of IMCs layer at the center of the interface changes from $FeAl_3$ with high brittleness to FeAl with high toughness, and the thickness of the IMCs layer decreased from 5.01 μm to 0.71 μm. The improvement of mechanical interlocking ability, the change of the type of IMCs layer, and the thinning of the IMC layer increase the failure load of the lap joint.

Credit authorship contribution statement

Tao Liu: Conceptualization, Resources, Writing - Original Draft, Writing - Review & Editing. **Song Gao:** Conceptualization, Resources, Writing - Original Draft, Writing - Review & Editing, Oversight and leadership, Project administration. **Weicheng Ye:** Conceptualization, Resources, Writing - Review & Editing. **Lei Shi:** Conceptualization, Resources, Oversight and leadership, Project administration. **Sachin Kumar:** Conceptualization, Resources, Writing - Review & Editing. **Junnan Qiao:** Conceptualization, Resources, Writing - Review & Editing.

Data availability

Data will be made available on request.

Declaration of Competing Interest

The authors declare that they have no known competing financial interests or personal relationships that could have appeared to influence the work reported in this paper.

Acknowledgement

This work was supported by the Natural Science Foundation of Shandong Province (ZR2020QE177) and the Program for the integration between industry and education of Qilu University of Technology (Shandong Academy of Sciences) (2022PX071).

REFERENCES

[1] Baek S, Go GY, Park JW, Song J, Lee HC, Lee SJ, et al. Microstructural and interface geometrical influence on the mechanical fatigue property of aluminum/high-strength steel lap joints using resistance element welding for lightweight vehicles: experimental and computational investigation. J Mater Res Technol 2022;17:658–78. https://doi.org/10.1016/j.jmrt.2022.01.041.

[2] Heidarzadeh A, Mironov S, Kaibyshev R, Çam G, Simar A, Gerlich A, et al. Friction stir welding/processing of metals and alloys: a comprehensive review on microstructural evolution. Prog Mater Sci 2020;117:100752. https://doi.org/10.1016/j.pmatsci.2020.100752.

[3] Ma YW, Lou M, Li YB, Lin ZQ. Effect of rivet and die on self-piercing rivetability of AA6061-T6 and mild steel CR4 of different gauges. J Mater Process Technol 2018;251:282–94. https://doi.org/10.1016/j.jmatprotec.2017.08.020.

[4] Wang T, Sidhar H, Mishra RS, Hovanski Y, Upadhyay P, Carlson B. Evaluation of intermetallic compound layer at aluminum/steel interface joined by friction stir scribe technology. Mater Des 2019;174:107795. https://doi.org/10.1016/j.matdes.2019.107795.

[5] Wang J, Ling X, Zhang W, Lu X, Chen C. Microstructures and mechanical properties of friction stir welded butt joints of 3003-H112 aluminum alloy to 304 stainless steel used in plate-fin heat exchanger. J Mater Res Technol 2022;21:3086–97. https://doi.org/10.1016/j.jmrt.2022.10.161.

[6] Tanaka T, Nezu M, Uchida S, Hirata T. Mechanism of intermetallic compound formation during the dissimilar friction stir welding of aluminum and steel. J Mater Sci 2020;55:3064–72. https://doi.org/10.1007/s10853-019-04106-2.

[7] Mishra RS, Ma ZY. Friction stir welding and processing. Mater Sci Eng R Rep 2005;50:1–78. https://doi.org/10.1016/j.mser.2005.07.001.

[8] Kar A, Vicharapu B, Morisada Y, Fujii H. Elucidation of interfacial microstructure and properties in friction stir lap welding of aluminium alloy and mild steel. Mater Char 2020;168:110572. https://doi.org/10.1016/j.matchar.2020.110572.

[9] Batistão BF, Bergmann LA, Gargarella P, Alcântara NG de, dos Santos JF, Klusemann B. Characterization of dissimilar friction stir welded lap joints of AA5083 and GL D36 steel. J Mater Res Technol 2020;9:15132–42. https://doi.org/10.1016/j.jmrt.2020.10.078.

[10] Geng P, Morimura M, Ma H, Ma Y, Ma N, Liu H, et al. Elucidation of intermetallic compounds and mechanical properties of dissimilar friction stir lap welded 5052 Al alloy and DP590 steel. J Alloys Compd 2022;906:164381. https://doi.org/10.1016/j.jallcom.2022.164381.

[11] Abd Elnabi MM, Osman TA, El Mokadem A, Elshalakany AB. Evaluation of the formation of intermetallic compounds at the intermixing lines and in the nugget of dissimilar steel/aluminum friction stir welds. J Mater Res Technol 2020;9:10209–22. https://doi.org/10.1016/j.jmrt.2020.07.027.

[12] Wu CH, Liu T, Gao S, Shi L, Liu HT. Ultrasonic vibration enhanced friction stir welding process of aluminum/steel

dissimilar metals. J Mater Eng 2022;50:33–42. https://doi.org/10.11868/j.issn.1001-4381.2021.000338.
[13] Rai R, De A, Bhadeshia HKDH, DebRoy T. Review: friction stir welding tools. Sci Technol Weld Join 2011;16:325–42. https://doi.org/10.1179/1362171811Y.0000000023.
[14] Shen Z, Chen Y, Haghshenas M, Gerlich AP. Role of welding parameters on interfacial bonding in dissimilar steel/aluminum friction stir welds. Eng Sci Technol an Int J 2015;18:270–7. https://doi.org/10.1016/j.jestch.2014.12.008.
[15] Wan L, Huang Y. Microstructure and mechanical properties of Al/steel friction stir lap weld. Metals 2017;7:1–14. https://doi.org/10.3390/met7120542.
[16] Helal Y, Boumerzoug Z, Fellah L. Microstructural evolution and mechanical properties of dissimilar friction stir lap welding aluminum alloy 6061-T6 to ultra low carbon steel. Energy Proc 2019;157:208–15. https://doi.org/10.1016/j.egypro.2018.11.182. Elsevier Ltd.
[17] Wei Y, Xiong J, Li J, Zhang F, Liang S. Microstructure and enhanced atomic diffusion of friction stir welding aluminium/steel joints. Mater Sci Technol 2017;33:1208–14. https://doi.org/10.1080/02670836.2016.1274464.
[18] Derazkola HA, Khodabakhshi F. Underwater submerged dissimilar friction-stir welding of AA5083 aluminum alloy and A441 AISI steel. Int J Adv Manuf Technol 2019;102:4383–95. https://doi.org/10.1007/s00170-019-03544-1.
[19] Eyvazian A, Hamouda A, Tarlochan F, Derazkola HA, Khodabakhshi F. Simulation and experimental study of underwater dissimilar friction-stir welding between aluminium and steel. J Mater Res Technol 2020;9:3767–81. https://doi.org/10.1016/j.jmrt.2020.02.003.
[20] Tang J, Shen Y. Effects of preheating treatment on temperature distribution and material flow of aluminum alloy and steel friction stir welds. J Manuf Process 2017;29:29–40. https://doi.org/10.1016/j.jmapro.2017.07.005.
[21] Liu X, Lan S, Ni J. Electrically assisted friction stir welding for joining Al 6061 to TRIP 780 steel. J Mater Process Technol 2015;219:112–23. https://doi.org/10.1016/j.jmatprotec.2014.12.002.
[22] Bang HS, Bang HS, Jeon GH, Oh IH, Ro CS. Gas tungsten arc welding assisted hybrid friction stir welding of dissimilar materials Al6061-T6 aluminum alloy and STS304 stainless steel. Mater Des 2012;37:48–55. https://doi.org/10.1016/j.matdes.2011.12.018.
[23] Huang Y, Huang T, Wan L, Meng X, Zhou L. Material flow and mechanical properties of aluminum-to-steel self-riveting friction stir lap joints. J Mater Process Technol 2019;263:129–37. https://doi.org/10.1016/j.jmatprotec.2018.08.011.
[24] Huang Y, Wang J, Wan L, Meng X, Liu H, Li H. Self-riveting friction stir lap welding of aluminum alloy to steel. Mater Lett 2016;185:181–4. https://doi.org/10.1016/j.matlet.2016.08.102.
[25] Thomä M, Wagner G, Straß B, Wolter B, Benfer S, Fürbeth W. Ultrasound enhanced friction stir welding of aluminum and steel: process and properties of EN AW 6061/DC04-Joints. J Mater Sci Technol 2018;34:163–72. https://doi.org/10.1016/j.jmst.2017.10.022.
[26] Hong K, Wang Y, Zhou J, Zhou C, Wang L. Investigation on ultrasonic assisted friction stir welding of aluminum/steel dissimilar alloys. High Temp Mater Process 2021;40:45–52. https://doi.org/10.1515/htmp-2021-0011.
[27] Liu X, Wu C, Padhy GK. Characterization of plastic deformation and material flow in ultrasonic vibration enhanced friction stir welding. Scripta Mater 2015;102:95–8. https://doi.org/10.1016/j.scriptamat.2015.02.022.
[28] Liu XC, Wu CS, Padhy GK. Improved weld macrosection, microstructure and mechanical properties of 2024Al-T4 butt joints in ultrasonic vibration enhanced friction stir welding. Sci Technol Weld Join 2015;20:345–52. https://doi.org/10.1179/1362171815Y.0000000021.
[29] Lv XQ, Wu CS, Padhy GK. Diminishing intermetallic compound layer in ultrasonic vibration enhanced friction stir welding of aluminum alloy to magnesium alloy. Mater Lett 2017;203:81–4. https://doi.org/10.1016/j.matlet.2017.05.090.
[30] Zhao J, Wu CS, Shi L. Effect of ultrasonic field on microstructure evolution in friction stir welding of dissimilar Al/Mg alloys. J Mater Res Technol 2022;17:1–21. https://doi.org/10.1016/j.jmrt.2021.12.133.
[31] Liu T, Gao S, Xiao GC, Wu CH, Shi L, Sun ZP. Process optimization on friction stir lap welding of 6061-T6 aluminum alloy/Q235 steel with ultrasonic vibration. Trans China Weld Inst 2022;43(5):69–75. https://doi.org/10.12073/j.hjxb.20220101007.
[32] Chitturi V, Pedapati SR, Awang M. Effect of tilt angle and pin depth on dissimilar friction stir lap welded joints of aluminum and steel alloys. Materials 2019;12:1–11. https://doi.org/10.3390/ma122333901.
[33] Gao S, Wu CS, Padhy GK, Shi L. Evaluation of local strain distribution in ultrasonic enhanced Al 6061-T6 friction stir weld nugget by EBSD analysis. Mater Des 2016;99:135–44. https://doi.org/10.1016/j.matdes.2016.03.055.
[34] Gao S, Wu CS, Padhy GK. Process and joint quality of ultrasonic vibration enhanced friction stir lap welding. Sci Technol Weld Join 2018;23:693–703. https://doi.org/10.1080/13621718.2018.1476084.
[35] Padhy GK, Wu CS, Gao S. Precursor ultrasonic effect on grain structure development of AA6061-T6 friction stir weld. Mater Des 2017;116:207–18. https://doi.org/10.1016/j.matdes.2016.11.108.
[36] Padhy GK, Wu CS, Gao S. Subgrain formation in ultrasonic enhanced friction stir welding of aluminium alloy. Mater Lett 2016;183:34–9. https://doi.org/10.1016/j.matlet.2016.07.033.
[37] Hu Y, Liu H, Fujii H, Ushioda K, Araki H, Sugita K, et al. Vacancy-induced θ′ precipitation during ultrasonic-affected friction stir welding of Al–Cu alloy. J Mater Sci 2020;55:14626–41. https://doi.org/10.1007/s10853-020-05061-z.
[38] Gao S, Wu CS, Padhy GK. Material flow, microstructure and mechanical properties of friction stir welded AA 2024-T3 enhanced by ultrasonic vibrations. J Manuf Process 2017;30:385–95. https://doi.org/10.1016/j.jmapro.2017.10.008.
[39] Pourali M, Abdollah-zadeh A, Saeid T, Kargar F. Influence of welding parameters on intermetallic compounds formation in dissimilar steel/aluminum friction stir welds. J Alloys Compd 2017;715:1–8. https://doi.org/10.1016/j.jallcom.2017.04.272.
[40] Sandnes L, Bergh T, Grong Ø, Holmestad R, Vullum PE, Berto F. Interface microstructure and tensile properties of a third generation aluminium-steel butt weld produced using the Hybrid Metal Extrusion & Bonding (HYB) process. Mater Sci Eng, A 2021:809. https://doi.org/10.1016/j.msea.2021.140975.
[41] Wan L, Huang Y. Friction stir welding of dissimilar aluminum alloys and steels: a review. Int J Adv Manuf Technol 2018;99:1781–811. https://doi.org/10.1007/s00170-018-2601-x.
[42] Azizieh M, Yazdi M, Tahmasebi M, Miraali M, Mashtizadeh A. Characteristics of dissimilar friction stir spot brazing between aluminum and galvanized steel. Mater Res Express 2019;6. https://doi.org/10.1088/2053-1591/aaec9d.
[43] Liu T, Gao S, Shen X, Sun Z, Shi L, Kumar S. Acoustic effect on the joint quality and process of friction stir lap welding of aluminum to steel. Mater Today Commun 2023;35:106184. https://doi.org/10.1016/j.mtcomm.2023.106184.